ELSEVIER

Chemical Engineering Journal 128 (2007) 115–125

Chemical Engineering Journal

www.elsevier.com/locate/cej

# Simulation of large-scale membrane reformers by a two-dimensional model

M. De Falco *, L. Di Paola, L. Marrelli, P. Nardella

*Chemical Engineering Department, University of Rome "La Sapienza", via Eudossiana, 18 00184 Roma, Italy*

Received 26 July 2006; received in revised form 6 October 2006; accepted 18 October 2006

**Abstract**

The effect of hydrogen removal in membrane reformers is analyzed by a two-dimensional, non-isothermal model. Unlike previous works, which refer to laboratory scale reactors and low space velocity of gas mixture, simulations carried out in the present work concern large-scale reactors (length $\simeq$ 12 m, diameter $\simeq$ 0.12 m) and high hydrogen productivity (volumetric flow rates within 50–130 $Nm^3/h$) involved in industrial applications. Results show that methane conversion is far from unity (about 37–50% dependently on operating conditions), even though larger than that one attainable in absence of membrane (∼28% at simulation conditions). The two-dimensional approach allows the radial distribution of temperature and hydrogen partial pressure to be shown. A lower removal rate of hydrogen than in the one-dimensional model is found due to the lower hydrogen partial pressure near the membrane surface. Finally, thermal level required from membrane reactors is lower than in traditional reformers, so that less demanding ovens and less expensive materials can be used.


*Keywords:* Methane steam reforming; Two-dimensional model; Hydrogen production; Membrane reactor

## 1. Introduction

Membrane reactors are becoming more and more interesting in processes where equilibrium conditions prevent high conversion of reactants to be achieved. Steam reforming of methane for production of hydrogen is the main field of research and application of this promising technology. The whole process is endothermic and occurs over a Ni-based catalyst in tubular reactors; equilibrium conditions are quickly reached but a significant hydrogen yield is achieved only at high temperature so that a great amount of heat is required. Tubular reactors are usually placed inside a furnace where the heat produced by combustion is transferred to the reacting gas through the reformer tube wall. In such a configuration, reformer tubes are subjected to large stresses since they operate at high temperature with large thermal gradient in axial and radial directions and the high pressure inside the tube could lead to creep rupture. Moreover, there is a risk of carbon formation on hot tube wall [1]. The use of membrane reactors (MR) appears to be a possible way to improve hydrogen yield at lower temperatures because the removal of hydrogen from the reaction environment prevents the equilibrium to be achieved. A large number of scientific papers and technical reports have appeared about the integration of membranes in steam reformers and several mathematical models have been presented and used to simulate the operation of these reactors. However, most of these works refer to small-scale reactors and use one-dimensional models which do not take into account radial temperature and composition gradients, while a proper representation of these gradients is essential to calculate the tube wall and membrane temperatures, the right driving force of hydrogen flux through the membrane and to assess the activity of the catalyst at the inner and colder position. Several one-dimensional models, both isothermal [2–5] and non-isothermal [6–10], can be found in the literature. Most of these models are used to simulate laboratory experiments and thus they are applied at reactor sizes and operating conditions (Table 1) where radial gradients are negligible.

At present, membrane reactor technology is not yet applied at, industrial scale to steam reforming; therefore, problems and advantages of this process cannot be deduced from industrial skills and its feasibility can be assessed only by theoretical simulations. Unfortunately, only few studies are reported in the literature and models used in simulations are sometimes based

* Corresponding author. Tel.: +39 6 44585704.
*E-mail address:* marcello.defalco@uniroma1.it (M. De Falco).

1385-8947/$ – see front matter © 2006 Elsevier B.V. All rights reserved.
doi:10.1016/j.cej.2006.10.021

**Nomenclature**

| | |
|---|---|
| $B_H$ | hydrogen permeability (kmol m$^{-1}$ h$^{-1}$ kPa$^{-0.5}$) |
| $c_i$ | molar concentration (kmol m$^{-3}$), $i$ = $CH_4$, $H_2O$, $H_2$, CO, $CO_2$ |
| $c_i^0$ | inlet molar concentration (kmol m$^{-3}$), $i$ = $CH_4$, $H_2O$. $H_2$, CO, $CO_2$ |
| $c_{p,m}$ | gas mixture specific heat (kJ kmol$^{-1}$ K$^{-1}$) |
| $c_{p,perm}$ | gas mixture specific heat in permeation zone (kJ kmol$^{-1}$ K$^{-1}$) |
| $c_{tot}$ | total concentration (kmol m$^{-3}$) |
| $d_{c,o}$, $d_{c,i}$, $h_c$ | catalyst particle dimensions (m) |
| $d_{eq}$ | equivalent reactor diameter (m) |
| $d_p$ | equivalent particle diameter (m) |
| $f$ | friction factor |
| $F_{CH_4}^{in}$ | inlet methane flow rate (kmol h$^{-1}$) |
| $F_{CH_4}^{out}$ | outlet methane flow rate (kmol h$^{-1}$) |
| $F_{CO_2}^{in}$ | inlet carbon dioxide flow rate (kmol h$^{-1}$) |
| $F_{CO_2}^{out}$ | outlet carbon dioxide flow rate (kmol h$^{-1}$) |
| $F_{H_2,perm}^{out}$ | outlet hydrogen flow rate in permeation zone (kmol h$^{-1}$) |
| $F_{P,tot}$ | total molar flow rate in permeation zone (kmol h$^{-1}$) |
| $F_{sweep}$ | sweeping gas flow rate in permeation zone (kmol h$^{-1}$) |
| $G$ | mass specific gas flow-rate (kg m$^{-2}$ h$^{-1}$) |
| $h_{P,H_2}$ | permeation zone hydrogen enthalpy (kJ kmol$^{-1}$) |
| $h_{R,H_2}$ | reaction zone hydrogen enthalpy (kJ kmol$^{-1}$) |
| $h_w$ | heat transport coefficient near wall (kJ m$^{-2}$ h$^{-1}$ K$^{-1}$) |
| $h_{w,p}$ | forced convection heat transport coefficient in permeation zone (kJ m$^{-2}$ h$^{-1}$ K$^{-1}$) |
| $\Delta H_{298}^{\circ}$ | standard reaction enthalpy (kJ mol$^{-1}$) |
| $H_2^{rec}/H_2^{prod}$ | hydrogen recovered on total hydrogen produced ratio |
| $-\Delta H_j$ | $j$th reaction enthalpy (kJ mol$^{-1}$) |
| $k_{mem}$ | membrane thermal conductivity (kJ m$^{-1}$ h$^{-1}$ K$^{-1}$) |
| $L$ | reactor length (m) |
| $N_m$ | hydrogen flux permeating through membrane (kmol m$^{-2}$ h$^{-1}$) |
| $p$ | emissivity of solid surface |
| $p_{H_2,perm}$ | hydrogen partial pressure in permeation zone (kPa) |
| $p_{H_2,reac}$ | hydrogen partial pressure in reaction zone (kPa) |
| $Pe_{mr}$ | mass effective radial Peclet number |
| $P_P$ | permeation zone pressure (kPa) |
| $P_P^{in}$ | inlet permeation zone pressure (kPa) |
| $P_R$ | reaction zone pressure (kPa) |
| $P_R^{in}$ | inlet reaction zone pressure (kPa) |
| $Pr$ | Prandtl number |
| $Pr_{perm}$ | Prandtl number in permeation zone |
| $q_m$ | heat flux from the reaction to the permeation zone (kW m$^{-2}$) |
| $q_r$ | axial heat flux (kW m$^{-2}$) |
| $Q_{TR}$ | heat duty in the traditional reactor (kW) |
| $Q_{MR}$ | heat duty in the membrane reactor (kW) |
| $Q_{H_2}$ | volumetric hydrogen flow-rate (Nm$^3$ h$^{-1}$) |
| $\tilde{r}$ | dimensionless radial coordinate |
| $r_{i,i}$ | internal tube internal radius (m) |
| $r_{o,i}$ | internal tube external radius (m) |
| $r_{i,o}$ | external tube internal radius (m) |
| $r_{o,o}$ | external tube external (m) |
| $R$ | gas universal constant (kJ kmol$^{-1}$ K$^{-1}$) |
| $R_j$ | kinetic rate of $j$th reaction (kmol kg$_{cat}^{-1}$ h$^{-1}$) |
| $Re_p$ | Reynolds number referred to the equivalent particle diameter ($G{\cdot}d_p/\mu_G$) |
| $Re_{perm}$ | Reynolds number in permeation zone |
| $T_{mem}$ | membrane temperature (K) |
| $T_P$ | permeation zone temperature (K) |
| $T_P^{in}$ | inlet permeation zone temperature (K) |
| $T_R$ | reaction zone temperature (K) |
| $T_R^{in}$ | inlet reaction zone temperature (K) |
| $T_{w,o}$ | external wall temperature (K) |
| $u_z$ | gas velocity (m h$^{-1}$) |
| $u_z^0$ | inlet gas velocity (m h$^{-1}$) |
| $U$ | overall heat transfer coefficient (outside and reaction zone) (kJ m$^{-2}$ h$^{-1}$ K$^{-1}$) |
| $U_1$ | overall heat transfer coefficient (reaction and permeation zone) (kJ m$^{-2}$ h$^{-1}$ K$^{-1}$) |
| $X_{CH_4}$ | methane conversion |
| $X_{CO_2}$ | carbon dioxide yield |
| $y_i^0$ | inlet mole fraction, $i$ = $CH_4$, $H_2O$, $H_2$, CO, $CO_2$ |
| $Y_{H_2}$ | hydrogen recovered per mole of methane |
| $\tilde{z}$ | dimensionless axial coordinate |

*Greek symbols*

| | |
|---|---|
| $\alpha_{met}$ | metal conductivity (kJ m$^{-2}$ h$^{-1}$ K$^{-1}$) |
| $\alpha_{ru}$, $\alpha_{rs}$ | parameters defined by Eq. (26) (kJ m$^{-2}$ h$^{-1}$ K$^{-1}$) |
| $\delta$ | membrane thickness (m) |
| $\epsilon$ | void fraction |
| $\eta$ | effectiveness factor |
| $\lambda_{er}$ | effective radial thermal conductivity (kJ m$^{-1}$ h$^{-1}$ K$^{-1}$) |
| $\lambda_{er}^0$ | static radial thermal conductivity (kJ m$^{-1}$ h$^{-1}$ K$^{-1}$) |
| $\lambda_g$ | gas phase thermal conductivity (kJ m$^{-1}$ h$^{-1}$ K$^{-1}$) |
| $\lambda_{g,perm}$ | gas phase thermal conductivity in permeation zone (kJ m$^{-1}$ h$^{-1}$ K$^{-1}$) |
| $\lambda_s$ | packing material thermal conductivity (kJ m$^{-1}$ h$^{-1}$ K$^{-1}$) |
| $\mu_g$ | gas mixture viscosity (kg m$^{-1}$ h$^{-1}$) |
| $\rho_{app}$ | apparent packing material density (kg m$^{-3}$) |
| $\rho_b$ | packed bed density (kg m$^{-3}$) |
| $\rho_g$ | gas mixture density (kg m$^{-3}$) |

Table 1
Geometric parameters and inlet methane flow-rates

| | $r_{i,o}$ (cm) | $r_{o,i}$ (cm) | $L$ (m) | $F^{in}_{CH_4}$ (kmol/h) |
|---|---|---|---|---|
| Shu et al. | 0.85 | 0.475 | 0.036 | $1.07 \times 10^{-4}$ |
| Lin et al. | – | 0.635 | 0.15 | $1.5 \times 10^{-3}$ |
| Gallucci et al. | – | – | – | $4.6 \times 10^{-5}$ |
| Oklany et al. | 0.5 | – | 0.1 | $2.68 \times 10^{-4}$ |
| Madia et al. | 2 | 1.25 | 0.17 | $4.93 \times 10^{-4}$ |
| Yu et al. | 8 | 4.5 | 1.2 | $1.28 \times 10^{-2}$ |

on assumptions, which do not allow important effects to be shown.

Fernandez and Soares [11] have used a non-isothermal, one-dimensional model to simulate the behaviour of a large-scale MR ($r_{i,o} = 0.0508$ m, $r_{o,i} = 0.01015$ m, $L = 20$ m). Some of their assumptions (pressure drop negligible, membrane permeability independent of the temperature) are questionable as for hydrogen flux through the membrane, but the main limit of their one-dimensional approach is the impossibility of accounting for radial differences, which could be not negligible in industrial reactors. Recently, Koukou et al. [12] have presented a two-dimensional model of a water gas shift ceramic membrane reactor: the model takes into account both axial and radial distributions of temperature and partial pressures. The results of simulations obtained by this model clearly show the effect of the radial gradient of hydrogen partial pressure which reduces driving force through the membrane and, consequently, the hydrogen flux towards the permeation side; of course, one-dimensional models that neglect this effect overestimate the reactor performance. Two-dimensional models have been used as well by Fukuhara and Igarashi [13] and Assabumrungrat et al. [14] in simulations of membrane reactors for dehydrogenation of ethylbenzene. However, a very small reactor is considered [14] or physical properties of gas mixture are assumed everywhere constant inside the reactor [13].

The aim of the present paper is to use two-dimensional models of industrial reformers in order to analyze axial and radial gradients of composition and temperature and to assess both technological and process problems, which could appear in large-scale equipments. Two models are presented: the membrane reactor (MR) two-dimensional model and the traditional reactor (TR) two-dimensional model. After some remarks about heat transfer between the external source and the reaction zone and between the reaction zone and permeation side, a comparison between TR and MR is done and advantages in introducing membranes in the reformer are discussed.

The effect of some operating conditions, such as permeation zone pressure, sweeping gas flow rate, reaction pressure and steam to carbon ratio, has been studied and some remarks have been made about their influence on reactions and permeation. Unlike most of works reported in the literature dealing with laboratory conditions, simulations are performed with reference to industrial cases: not trivial differences are found.

## 2. Mathematical model

The main reactions taken into account in modelling steam-reforming reactors are:

$$CH_4 + H_2O \Leftrightarrow CO + 3H_2 \qquad \Delta H^{\circ}_{298} = 206\,\text{kJ/mol} \tag{1}$$

$$CO + H_2O \Leftrightarrow CO_2 + H_2 \qquad \Delta H^{\circ}_{298} = -41\,\text{kJ/mol} \tag{2}$$

$$CH_4 + 2H_2O \Leftrightarrow CO_2 + 4H_2 \qquad \Delta H^{\circ}_{298} = 165\,\text{kJ/mol} \tag{3}$$

Secondary reactions, as carbon formation, are not considered.

Models are based on mass, energy and momentum balances together with the intrinsic kinetic equations reported by Xu and Froment [15].

The TR is a conventional packed tube while the MR consists of two concentric tubes, where the inner one is the membrane through which hydrogen permeates and the outer is the reactor shell.

The following assumptions have been made:

- steady-state conditions;
- negligible axial dispersion and radial convective terms;
- ideal gas behaviour;
- a single tube representative of any other tube;
- a single pseudo-effectiveness factor independent of reaction and of local conditions;
- permselectivity of the membrane towards hydrogen 100%.

The effectiveness factor $\eta$, defined as known as the ratio between the observed reaction rate and the reaction rate calculated at external catalytic surface conditions (or at bulk fluid conditions in absence of external mass transport resistance), depends on temperature and fluid composition, which change in radial and axial direction. Analytical expressions of $\eta$ are very useful to evaluate effective reaction rate to be used in mass balances. Unfortunately, in the presence of multiple reactions, the problem is very complex and the evaluation of observed reaction rates requires to find concentration profiles inside catalyst particles taking into account the presence of many diffusing species and many reactions. In spite of this, a pseudo-effectiveness factor $\eta$, independent of local conditions, is used in this work. This approach has to be considered only an arbitrary way to reduce the real reaction rate with respect to the value given by the intrinsic kinetics. Rostrup-Nielsen [16] have evaluated $\eta$ values below 0.1; Xu and Froment [17] suggest $\eta = 0.02$ as an average realistic value. In this work $\eta$ is taken equal to 0.02.

Equations of TR and MR models, together with boundary conditions, are reported as follows:

- TR model:
  - Mass balances for all components: $i = CH_4$, $H_2O$, $H_2$, CO, $CO_2$:

$$\frac{\partial(u_z \cdot c_i)}{\partial \tilde{z}} = \frac{d_p \cdot L}{Pe_{mr} \cdot r^2_{i,o}} \cdot \left( \frac{\partial^2(u_z \cdot c_i)}{\partial \tilde{r}^2} + \frac{1}{\tilde{r}} \cdot \frac{\partial(u_z \cdot c_i)}{\partial \tilde{r}} \right) - \eta \cdot \rho_b \cdot L \cdot \sum_j R_j \tag{4}$$

- Energy balance in reaction zone:

$$\frac{\partial T_R}{\partial \tilde{z}} = \frac{\lambda_{er} \cdot L}{(u_z \cdot c_{tot}) \cdot c_{p,m} \cdot r_{i,o}^2} \cdot \left( \frac{\partial^2 T_R}{\partial \tilde{r}^2} + \frac{1}{\tilde{r}} \cdot \frac{\partial T_R}{\partial \tilde{r}} \right) + \frac{\eta \cdot \rho_b \cdot L \cdot \sum_j (-\Delta H_j) \cdot R_j}{(u_z \cdot c_{tot}) \cdot c_{p,m}} \quad (5)$$

- Momentum balance in reaction zone:

$$\frac{dP_R}{d\tilde{z}} = \frac{f \cdot G \cdot \mu_g \cdot L}{\rho_g \cdot d_P^2} \cdot \frac{(1-\epsilon)^2}{\epsilon^3} \quad (6)$$

- Boundary conditions:

$$\tilde{z} = 0 \rightarrow \begin{cases} X_{CH_4} = X_{CO_2} = 0 \\ T_R = T_R^{in} \\ P_R = P_R^{in} \end{cases} \quad (7)$$

$$\tilde{r} = 0 \rightarrow \begin{cases} \dfrac{\partial X_{CH_4}}{\partial \tilde{r}} = \dfrac{\partial X_{CO_2}}{\partial \tilde{r}} = 0 \\ \dfrac{\partial T_R}{\partial \tilde{r}} = 0 \end{cases} \quad (8)$$

$$\tilde{r} = 1 \rightarrow \begin{cases} \dfrac{\partial X_{CH_4}}{\partial \tilde{r}} = \dfrac{\partial X_{CO_2}}{\partial \tilde{r}} = 0 \\ \lambda_{er} \cdot \dfrac{\partial T_R}{\partial \tilde{r}} = q_r = U \cdot (T_{w,o} - T_{R|r_{i,o}}) \end{cases} \quad (9)$$

- MR model:
  - Mass balances for all components: $i = CH_4, H_2O, H_2, CO, CO_2$:

$$\frac{\partial (u_z \cdot c_i)}{\partial \tilde{z}} = \frac{d_p \cdot L}{Pe_{mr} \cdot r_{i,o}^2} \cdot \left( \frac{\partial^2 (u_z \cdot c_i)}{\partial \tilde{r}^2} + \frac{1}{\tilde{r}} \cdot \frac{\partial (u_z \cdot c_i)}{\partial \tilde{r}} \right) - \eta \cdot \rho_b \cdot L \cdot \sum_j R_j \quad (10)$$

  - Energy balance in reaction zone:

$$\frac{\partial T_R}{\partial \tilde{z}} = \frac{\lambda_{er} \cdot L}{(u_z \cdot c_{tot}) \cdot c_{p,m} \cdot r_{i,o}^2} \cdot \left( \frac{\partial^2 (T_R)}{\partial \tilde{r}^2} + \frac{1}{\tilde{r}} \cdot \frac{\partial T_R}{\partial \tilde{r}} \right) + \frac{\eta \cdot \rho_b \cdot L \cdot \sum_j (-\Delta H_j) \cdot R_j}{(u_z \cdot c_{tot}) \cdot c_{p,m}} \quad (11)$$

  - Momentum balance in reaction zone:

$$\frac{dP_R}{d\tilde{z}} = \frac{f \cdot G \cdot \mu_g \cdot L}{\rho_g \cdot d_P^2} \cdot \frac{(1-\epsilon)^2}{\epsilon^3} \quad (12)$$

  - $H_2$ mass balance in permeation zone:

$$\frac{dY_{H_2}}{d\tilde{z}} = \frac{N_m \cdot 2\pi \cdot r_{o,i} \cdot L}{F_{CH_4}^{in}} \quad (13)$$

  - Energy balance in permeation zone:

$$\frac{dT_P}{d\tilde{z}} = \frac{L}{F_{P,tot} \cdot c_{p,perm}} \cdot (U_1 \cdot 2\pi \cdot r_{i,i} \cdot (T_R - T_P) + N_m \cdot \pi \cdot r_{o,i} \cdot (h_{R,H_2} - h_{P,H_2})) \quad (14)$$

  - Boundary conditions:

$$\tilde{z} = 0, \quad \vee \tilde{r} \rightarrow \begin{cases} u_z \cdot c_i = u_z^0 \cdot c_i^0 \\ T_R = T_R^{in} \\ P_R = P_R^{in} \\ Y_{H_2} = 0 \\ T_P = T_P^{in} \end{cases} \quad (15)$$

$$\tilde{r} = \tilde{r}_{i,o}, \quad \vee \tilde{z} \rightarrow \begin{cases} \dfrac{\partial (u_z \cdot c_i)}{\partial \tilde{r}} = 0 \\ \lambda_{er} \cdot \dfrac{\partial T_R}{\partial \tilde{r}} = q_r = U \cdot (T_{w,o} - T_{R|r_{i,o}}) \end{cases} \quad (16)$$

$$\tilde{r} = \tilde{r}_{o,i}, \quad \vee \tilde{z} \rightarrow \begin{cases} \dfrac{\partial (u_z \cdot c_i)}{\partial \tilde{r}} = 0 \quad (i = CH_4, H_2O, CO, CO_2) \\ \dfrac{d_p}{Pe_{mr}} \cdot \dfrac{\partial (u_z \cdot c_{H_2})}{\partial \tilde{r}} = N_m \\ \lambda_{er} \cdot \dfrac{\partial T_R}{\partial \tilde{r}} = q_m = U_1 \cdot (T_{R|r_{o,i}} - T_P) \end{cases} \quad (17)$$

In MR permeation zone, an isobaric one-dimensional model is used. In momentum balances, the friction factor is calculated by using Ergun model:

$$f = 150 + 1.75 \cdot \frac{Re_p}{1-\epsilon} \quad (18)$$

$Pe_{mr}$ is the mass effective radial Peclet number. Since, in a packed bed operating at industrial conditions, $Re$ is surely greater than 1000, $Pe_{mr}$ reaches the following constant value depending only on geometric features [18]:

$$Pe_{mr} = 8.8 \cdot \left[ 2 - \left( 1 - \frac{2 \cdot d_p}{d_{eq}} \right)^2 \right] \quad (19)$$

where $d_{eq}$ is the tube inner diameter of TR or the diameter of a circular cross-section equivalent to the annular section in the case of MR. In our simulations, TR and MR reactors are assumed to have the same cross-section of reacting zone so that the value of $d_{eq}$ is the same both for MR and TR.

All physical properties of the gas mixture are evaluated at local conditions. To this aim, equations reported by Sandler [19] have been used to calculate specific heats of pure components whereas viscosities have been taken from [20]; gas mixture viscosity has been evaluated as suggested by [21]; gas heat thermal conductivity, which is needed in effective radial thermal conductivity $\lambda_{er}$, is calculated by Wassiljewa equation [21–23].

### 2.1. Heat transport phenomena

Due to the strongly endothermic nature of the process, a large amount of heat has to be supplied in order to fulfil the energy absorbed by reactions. If the heat is supplied by an external source, a sequence of resistances controls heat flux from the furnace chamber to the reaction zone.

In mathematical models, two overall heat transfer coefficients, $U$ and $U_1$, appear: the first one, which appears in Eqs. (9) and (16), accounts for the resistances due to the stainless steel tube ($l/\alpha_{met}$) and for the layer in the immediate neighbourhood of the tube wall ($1/h_w$):

$$U = \left(\frac{1}{h_w} + \frac{1}{\alpha_{met}}\right)^{-1} \tag{20}$$

As explained by Tsotsas and Schlünder [24], the wall heat transfer coefficient $h_w$ has two possible meanings depending on the value of $Pe$ number. In the case of an industrial reactor, where the fluid-dynamic conditions are surely in the region of high $Pe$, the coefficient $h_w$ represents the conductivity of an "unmixed layer" where heat transport occurs only by molecular conduction. Several different correlations are proposed in the literature to evaluate $h_w$. In the present work, Li–Finlayson correlation is used [25]:

$$h_w = 0.17 \cdot \frac{\lambda_g}{d_p} \cdot \left(\frac{Pr}{0.7}\right)^{1/3} \cdot Re_p^{0.79} \tag{21}$$

The above expression is obtained as the best correlation of many experimental data for spherical particle beds in the region $0.05 < d_p/d_{eq} < 0.3$ and $20 < Re_p < 7600$.

The other overall heat transfer coefficient $U_1$ appears in Eq. (17) and represents the sum of heat resistances between reaction and permeation zone: it is given by the following expression:

$$U_1 = \left[\frac{1}{h_w} + \frac{\delta}{k_{mem}} + \frac{r_{o,i}}{r_{i,i}} \cdot \frac{1}{h_{w,p}}\right]^{-1} \tag{22}$$

where $h_w$ is the heat transfer coefficient corresponding to the membrane wall, $\delta$ and $k_{mem}$ are membrane thickness and thermal conductivity, respectively, and $h_{w,p}$ is the forced convection heat transport coefficient in the permeation zone given by (turbulence conditions) [26]:

$$h_{w,p} = \frac{\lambda_{g,perm}}{r_{i,i}} \cdot 0.023 \cdot Re_{perm}^{0.8} \cdot Pr_{perm}^{1/3} \tag{23}$$

Thermal and physical properties in Eq. (23) are calculated at permeation zone conditions (only sweep gas and hydrogen).

The effective radial thermal conductivity of catalyst bed $\lambda_{er}$ is obtained using the expression reported by [27,28] which assume the bed as a pseudo homogenous phase composed by catalyst particles and gas mixture:

$$\lambda_{er} = \lambda_{er}^0 + 0.111 \cdot \lambda_g \cdot \frac{Re_p \cdot Pr^{1/3}}{1 + 46 \cdot (d_p/d_{eq})^2} \tag{24}$$

In Eq. (24), $\lambda_{er}^0$ is the static contribution of the effective conductivity [29,30], i.e. the thermal conductivity of catalytic bed in absence of fluid flow:

$$\lambda_{er}^0 = \epsilon(\lambda_g + 0.95 \cdot \alpha_{ru} \cdot d_p) + \frac{0.95 \cdot (1-\epsilon)}{(2/3 \cdot \lambda_s) + (1/(10 \cdot \lambda_g + \alpha_{rs} \cdot d_p))} \tag{25}$$

$$\alpha_{ru} = \frac{0.8171 \cdot (T/100)^3}{1 + (\varepsilon/(2 \cdot (1-\varepsilon))) \cdot ((1-p)/p)}$$
$$\alpha_{rs} = 0.8171. \left(\frac{p}{2-p}\right) \cdot \left(\frac{T}{100}\right)^3 \tag{26}$$

In Eqs. (25) and (26), $p$ is the emissivity of solid surface, taken equal to 0.8 in our case, and $\lambda_s$ is the thermal conductivity of packing material, taken equal to 1.256 kJ/mhK for Ni-based catalyst. [28],

### 2.2. Membrane permeability

In MR, model, the flux of hydrogen through the membrane (see Eqs. (13), (14) and (17)) is calculated as follows:

$$N_m = \frac{B_H}{\delta} \cdot (p_{H_2,reac}^n - p_{H_2,perm}^n) \tag{27}$$

The value of the exponent $n$ depends on the thickness of Pd-based membrane. Shu et al. [2] report a variety of reasons to explain such behaviour. Probably, the transport mechanism changes with increasing $\delta$. If thickness is thin (few μm) the mass transport mechanism through membrane is controlled by the dissociative adsorption of hydrogen on Pd and $n$ is equal to 1, whereas if membrane is thicker (dozens of μm) the limiting step is diffusion of atomic H in the dense metallic layer and the flux follows the Sievert law with an exponent $n$ equal to 0.5. There is a region of thickness values where $n$ varies from 0.5 to 1 [31].

In the present work, the exponent $n$ is taken equal to 0.5 for two main reasons:

(1) in industrial MR, thin membranes should be avoided;
(2) it is preferable to test the membrane model in preservative conditions.

Depending on composition of the membrane, different expressions are reported in the literature to calculate the permeability $B_H$ [7,31,32]. In the present work, the expression given by Shu et al. [33] for Pd–Ag (5.1 wt.%)/porous SS membrane, is used:

$$B_H = 7.92 \times 10^{-5} \cdot \exp\left(-\frac{15700}{R \cdot T_{mem}}\right) \tag{28}$$

The membrane thickness is 20 μm. Eq. (28) shows a strong (exponential) effect of the temperature on membrane permeability; but temperature affects positively also the driving force of hydrogen flux across the membrane. Because of endothermic nature of reforming reaction, high conversions of methane and thus high hydrogen partial pressures are obtained at high temperatures with an improvement in the flux (see Eq. (27)). However, reaction temperature has to be limited due to technological properties and stability of the membrane.

### 2.3. Numerical solution

In order to solve the system of partial differential equations, the radial coordinate is made discrete by means of central

second-order differences: the resulting ODE system is solved using a Runge–Kutta method with variable step.

A profile of the supplied heat flux ($q_r$) is imposed as input in Eqs. (9) and (16): the external wall temperature is calculated from $q_r$ when temperatures inside the reactor are known. The membrane temperature and consequently the value of permeability is calculated step by step.

Reactor performance is evaluated through the following quantities:

$$X_{CH_4} = \frac{F^{in}_{CH_4} - F^{out}_{CH_4}}{F^{in}_{CH_4}} \quad \text{(methane conversion)}$$

$$X_{CO_2} = \frac{F^{out}_{CO_2} - F^{in}_{CO_2}}{F^{in}_{CH_4}} \quad \text{(carbon dioxide yield)}$$

$$Y_{H_2} = \frac{F^{out}_{H_2,perm}}{F^{in}_{CH_4}}$$

(hydrogen recovered per mole of methane (for MR only))

## 3. Results and discussion

TR and MR models reported above have been used to compare the two configurations at large scale. Since membrane steam reformers are not yet used at industrial scale, the comparison is carried out via simulation. Geometric and operating conditions typical of traditional steam reforming industrial plants are reported in Tables 2 and 3 and used in simulating a reference case. MR is assumed to be a bundle of parallel tubes, similar to TR used in industry: the behaviour of a single tube is considered to be representative of the behaviour of any other tube. Geometric sizes in MR are assigned in order to have the same section area in the two reformers (TR full section area = MR annular section area). A typical thickness value adopted for industrial reformer tubes has been used in fixing the external diameter of the reactor, whereas the membrane tube internal diameter comes from a (membrane + support) thickness (1 cm) able to support trans-membrane pressure differences and from a cross area to allow the sweeping gas (about 20 kmol/h) to flow inside without great pressure drops.

Table 2
Geometric conditions

| | TR | MR |
|---|---|---|
| $L$ (m) | 12 | 12 |
| $r_{o,o}$ (m) | 0.076 | 0.0875 |
| $r_{i,o}$ (m) | 0.063 | 0.0775 |
| $r_{o,i}$ (m) | – | 0.045 |
| $r_{i,i}$ (m) | – | 0.035 |
| $\delta$ (μm) | – | 20 |
| Catalyst properties | | |
| $\rho_{app}$ (kg/m$^3$) | 1990.6 | 1990.6 |
| $d_{c,o}$ (m) | 0.016 | 0.016 |
| $d_{c,i}$ (m) | 0.006 | 0.006 |
| $h_c$ (m) | 0.016 | 0.016 |
| $\epsilon$ | 0.5 | 0.5 |
| $\eta$ | 0.02 | 0.02 |

Table 3
Inlet operating conditions

| | |
|---|---|
| $T^{in}_R$ (K) | 773 |
| $P^{in}_R$ (kPa) | 2929 |
| $T^{in}_P$ (K) | 773 |
| $P^{in}_P$ (kPa) | 1010 |
| $F^{in}_{CH_4}$ (kmol/h) | 5 |
| $y^0H_2O$ | 0.7258 |
| $y^0H_2$ | 0.034 |
| $y^0CO$ | 0.0023 |
| $y^0CO_2$ | 0.0113 |
| $F_{sweep}$ (kmol/h) | $4 \cdot F^{in}_{CH_4}$ |

The heat flux supplied from outside has to be assigned as a function of axial coordinate: in simulations reported here, it is assumed to be constant along the reactor and its value in each reactor is such that the heat duty provided to TR and MR is the same; since the shell surface of MR is larger than that of TR, the heat flux is lower in MR.

A critical point is to maintain the membrane temperature at moderate values because of problems of thermal instability; for this reason heat fluxes of 20 kW/m$^2$ for MR and 24.6 kW/m$^2$ for TR, well below typical values used in industrial TR (about 80 kW/m$^2$ [1]), have been assumed as starting point of our simulations.

Fig. 1 shows methane conversion and carbon dioxide yield for MR and TR and the axial profile of temperature averaged in the section. The use of the membrane improves the reformer performance of about 33.1% in methane conversion (from 0.278 to 0.37) and 54.2% in $CO_2$ yield (from 0.23 to 0.354). This effect requires a greater quantity of energy for the reaction (the global process is endothermic) but, since supplied heat has been assumed to be the same in both reactors, a lower temperature is achieved in MR (exit temperature is about 837 K for MR versus 910.5 K for TR).

The improvement in methane conversion results from the higher reaction rate due to hydrogen removal from the reaction zone. In Fig. 2, axial profiles of methane reaction rate are depicted at different radial positions. In both TR and MR configuration, steam reforming reaction is quite fast near the hot wall, while in the tube core the reaction is slower due to the lower value of the temperature; however, the MR configuration is a little more efficient since the reaction rate is supported by the removal of $H_2$ near the membrane.

At conditions shown in Tables 2 and 3, hydrogen recovered per mole of methane $Y_{H_2}$ is 1.102 and 68.7% of hydrogen actually produced; a further separation step could be necessary to recover the hydrogen outgoing from the reaction zone together with the gas mixture, otherwise the output mixture, which has a high heating value, can be burned to give the heat duty necessary for the reaction and to produce steam required in reaction and permeation zone. The improvement of MR performance is more evident at higher hydrogen fluxes and, consequently, at higher driving forces. In Fig. 3, radial profiles of hydrogen partial pressure are shown for different axial

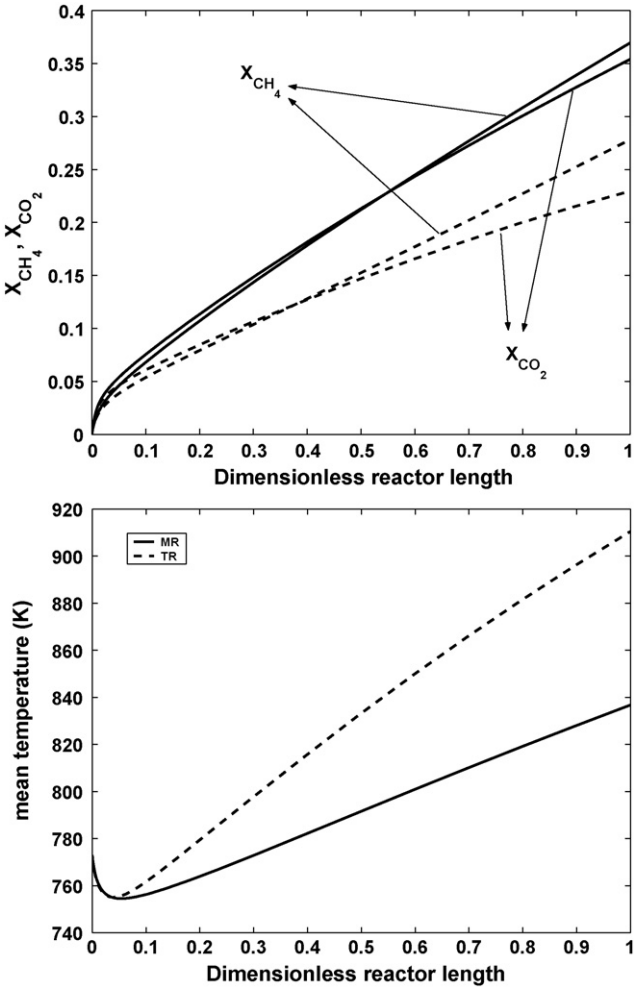


Fig. 1. Methane conversion, carbon dioxide yield and radial mean temperature in the reaction zone for TR (dashed line) and MR (solid line) at conditions reported in Tables 2 and 3.

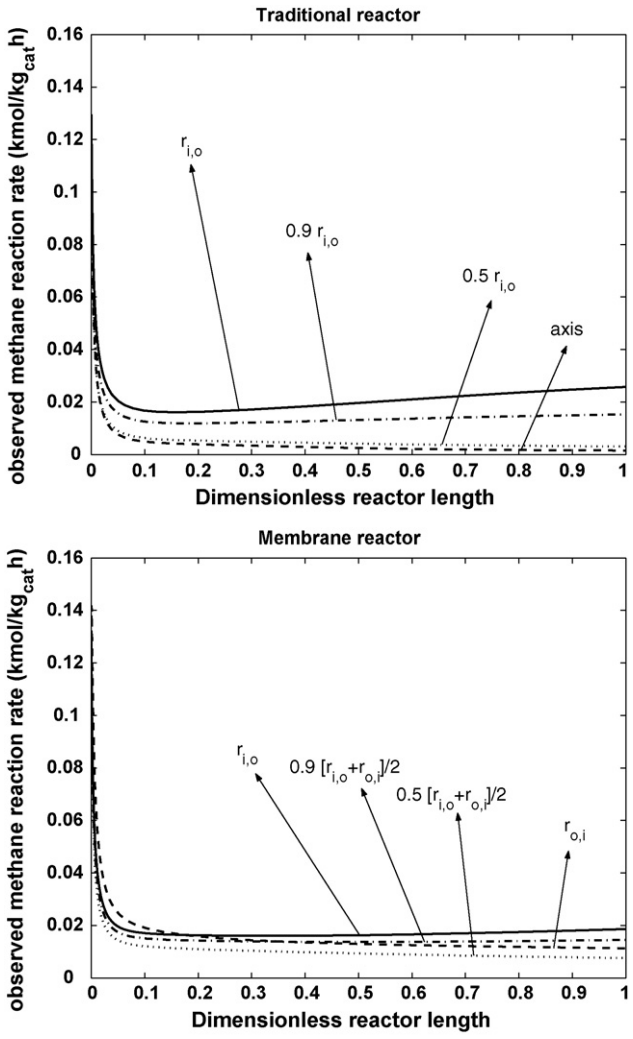


Fig. 2. Axial profiles of methane reaction rate at different radial position for TR and MR.

positions: near the membrane, $p_{H_2}$ is lower than the mean value in the section. Clearly, one-dimensional models, which cannot foresee these profiles, overestimate the hydrogen flux and the reactor performance: a quantitative comparison was performed between results obtained by two-dimensional and one-dimensional models at the same geometric and operating conditions (see Tables 2 and 3). Results are summarized in Table 4, where $Q_{H_2}$ is the outlet volumetric hydrogen flow rate in permeation zone (i.e. the recovered hydrogen) and $H_2^{rec}/H_2^{prod}$ indicates the percentage of hydrogen recovered on

Table 4
Comparison between results provided by 2D and 1D models (geometric parameters and operating conditions are those of Tables 2 and 3)

| | 2D model | 1D model |
|---|---|---|
| $Q_{H_2}$ (Nm$^3$/h) | 123.5 | 129.2 |
| $X_{CH_4}$ | 0.37 | 0.377 |
| $X_{CO_2}$ | 0.354 | 0.362 |
| $Y_{H_2}$ | 1.102 | 1.15 |
| $H_2^{rec}/H_2^{prod}$ | 68.7 | 70.2 |

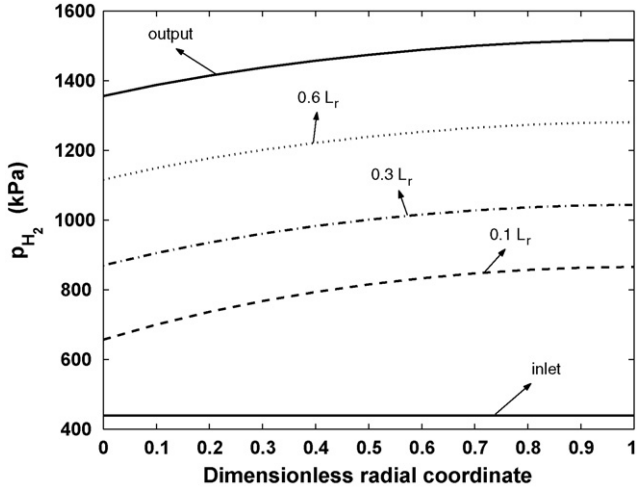


Fig. 3. Hydrogen partial pressure in radial direction (0 is near membrane, 1 is near tube wall) at different axial positions.

Table 5
Heat duty for TR and MR

| $X_{CH_4}$ | $Q_{TR}$ (kW) | $Q_{MR}$ (kW) | Heat duty saving (%) |
|---|---|---|---|
| 0.3 | 136 | 85.8 | 37 |
| 0.4 | 184.7 | 130.2 | 29.5 |
| 0.5 | 233.8 | 174.7 | 25.3 |
| 0.6 | 282.5 | 218.4 | 22.7 |
| 0.7 | 333.3 | 263.7 | 20.9 |

total produced. Actually, one-dimensional model overestimates hydrogen permeation flux and consequently, methane and carbon dioxide conversion: the size of over estimation is slight but not unimportant (4.6% in terms of $Q_{H_2}$).

In order to estimate the real benefit in using MR, total heat duty is calculated for both MR and TR fixing the outlet methane conversion: clearly, larger methane conversions require larger total heat duties, both in TR and MR. As shown in Table 5, $Q_{MR}$ is always smaller than $Q_{TR}$, but, when methane conversion increases, heat duty saving in MR reduces, so that the lower outlet conversion, the more advantageous MR becomes [33]. Moreover, since heat should be added at lower temperature in MR than TR, exergy efficiency is higher in MR. At high conversions, and consequently at high thermal duties, membrane temperature could reach unacceptable values; the membrane has a technological threshold, due to the thermal instability of material and adhesion problems between active compound and support. Maximum membrane temperature reached for each total supplied heat, and therefore, for each obtained methane conversion, is reported in Fig. 4. If the limit value of the allowed membrane temperature is fixed at 873 K, the maximum conversion that can be attained is 0.5 (Fig. 4). There is a technological threshold for TR too, that is the tube wall maximum temperature [16,34,35], normally fixed at 1200 K: at this limit the methane conversion is about 0.5 too, but the heat duty is much larger.

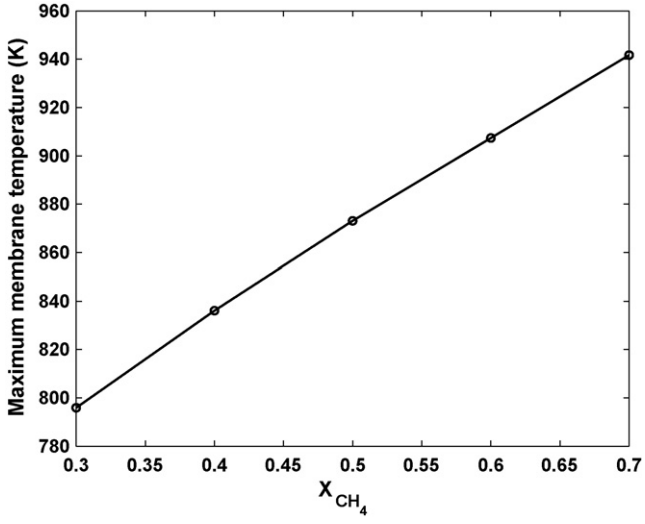


Fig. 4. Maximum membrane temperature for different outlet methane conversion.

Table 6
Effect of permeation zone pressure on some process quantities

| $P_P$ (kPa) | $X_{CH_4}$ | $X_{CO_2}$ | $Y_{H_2}$ | $H_2^{rec}/H_2^{prod}$ | $T_{m,max}$ (K) |
|---|---|---|---|---|---|
| 2929 | 0.32 | 0.293 | 0.635 | 46.2 | 855.4 |
| 1515 | 0.35 | 0.33 | 0.932 | 61.2 | 836.6 |
| 909 | 0.375 | 0.36 | 1.14 | 70.4 | 821.1 |
| 606 | 0.393 | 0.382 | 1.29 | 76 | 809.5 |
| 303 | 0.42 | 0.414 | 1.496 | 82.6 | 792 |
| 151.5 | 0.444 | 0.441 | 1.657 | 86.8 | 777.5 |

### 3.1. Effect of permeation zone operating conditions

The performance of MR can be improved reducing the permeation zone pressure, since a higher driving force has a positive effect on hydrogen removal and, consequently, on methane conversion. In Table 6, $X_{CH_4}$, $X_{CO_2}$, $Y_{H_2}$, the ratio between recovered and produced hydrogen and maximum membrane temperature are reported at different permeation zone pressures. The results in the first row correspond to the case in which the permeation zone pressure is equal to reaction zone pressure: the gain in methane conversion with respect to TR is only 22%. On the contrary, if pressure in the permeation zone is lowered to 1.5 bar, the gain reaches 69.5% and all the other quantities representing the quality of separation improve. Moreover, membrane temperature decreases since the larger heat requirement for the reactions reduces the reactor temperature.

However, pressure cannot be reduced too much in permeation zone for two main reasons:

(1) mechanical stress and shape loss of the membrane due to the difference between pressure in reaction and permeation zone;
(2) cost of hydrogen recompression for storage or for other applications.

Another way to improve MR performance is to get high driving force increasing sweeping gas flow-rate at permeation zone pressure constant (10 bar): increasing the ratio between sweeping gas and inlet methane flow rate from 3 to 12, $X_{CH_4}$ changes from 0.36 to 0.412 and the rate of hydrogen recovered on total hydrogen produced increases from 64.6% to 80.6%. However, sweeping flow rates up to 60 kmol/h are required, which is too much for a single tube and for $H_2$ dilution problems. In above simulations, sweeping gas has been assumed to be steam due to its easiness of separation from hydrogen; water vapour physical properties are, then, used in calculating heat transfer coefficient. Some differences in simulation results could be obtained using a different sweeping gas.

### 3.2. Effect of reaction zone pressure

The reaction zone pressure has opposite effects on MR performance: low pressure promotes equilibrium conversion but, at the same time, reduces the hydrogen flux through membrane. In Fig. 5, the effect of reaction pressure on methane conversion is shown for TR and MR at operating conditions reported in

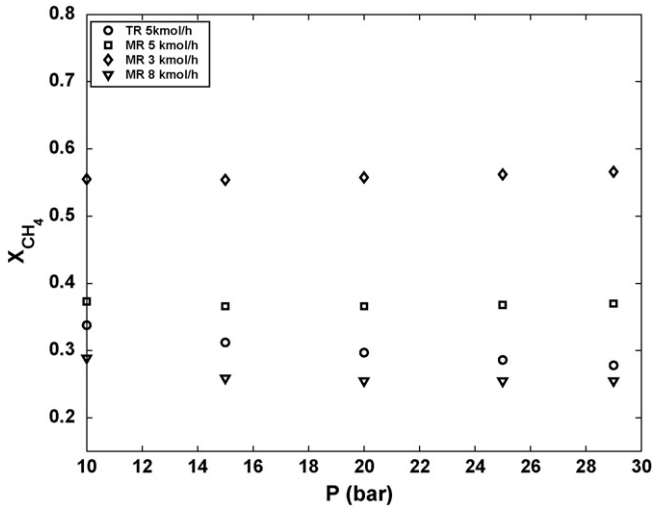


Fig. 5. Methane conversion vs. reaction zone pressure at different inlet flow rates.

Table 3; in the case of MR, $X_{CH_4}$ versus $P$ curves are shown as well at inlet methane flow rates of 3 kmol/h and 8 kmol/h. In the case of TR, a negative effect of $P$ on methane conversion can be observed due to thermodynamic reasons and to the longer residence time, resulting at the lower volumetric flow rates produced by high pressure.

On the other hand, in the case of MR, methane conversion is almost independent of $P$, since the negative effect on the reaction is redressed by the positive effect on permeation flux; the gain attainable by a membrane reactor is more evident at high pressure. Finally, short residence times correspond to large inlet flow rates with strong negative effects on reactor performance.

The profiles obtained (Fig. 5) are very similar to those reported by [36] for high space velocities which are typical of industrial reformers. In Table 7, the effect of pressure on pure hydrogen flow rate and on the percentage recovered is shown

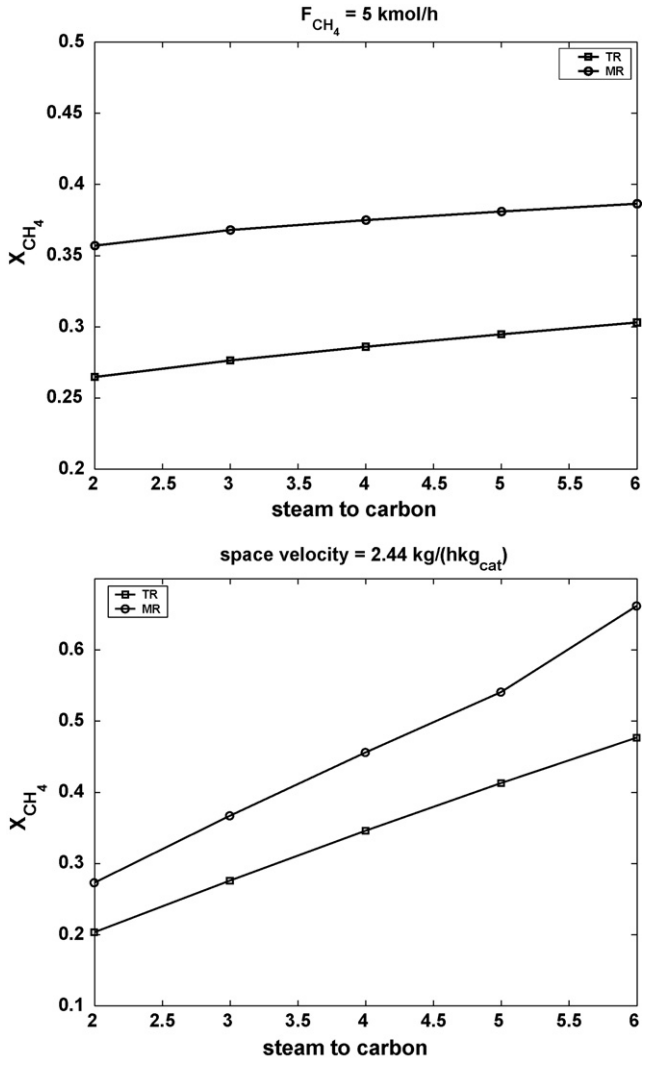


Fig. 6. Effect of S/C ratio at fixed molar flow rate and space velocity.

Table 7
Volumetric $H_2$ flow rates and recovered percentage for different pressure and inlet flow rates

| $P$ (bar) | 3 kmol/h | | 5 kmol/h | | 8 kmol/h | |
|---|---|---|---|---|---|---|
| | $Q_{H_2}$(Nm$^3$/h) | $H_2^{rec}/H_2^{prod}$ (%) | $Q_{H_2}$(Nm$^3$/h) | $H_2^{rec}/H_2^{prod}$ (%) | $Q_{H_2}$(Nm$^3$/h) | $H_2^{rec}/H_2^{prod}$ (%) |
| 10 | 67.8 | 44.8 | 67.74 | 37.7 | 48 | 20.7 |
| 15 | 87.6 | 57.5 | 90.6 | 51 | 91.6 | 43.5 |
| 20 | 101.1 | 65.6 | 105.5 | 59.4 | 110.6 | 53.1 |
| 25 | 111 | 71.1 | 116.5 | 65.2 | 123.7 | 59.5 |
| 29 | 117.3 | 74.4 | 123.5 | 68.7 | 131.87 | 63.3 |

Table 8
Effect of S/C recovered at fixed methane inlet flow rate and fixed space velocity

| $F_{CH_4}$ = 5 kmol/h | | | Space velocity = 2.45 kg/(h kg$_{cat}$) | | |
|---|---|---|---|---|---|
| S/C | $Q_{H_2}$(Nm$^3$/h) | $H_2^{rec}/H_2^{prod}$ (%) | S/C | $Q_{H_2}$(Nm$^3$/h) | $H_2^{rec}/H_2^{prod}$ (%) |
| 2 | 132.2 | 76.5 | 2 | 127.5 | 69.8 |
| 3 | 125 | 69.9 | 3 | 124.9 | 69.8 |
| 4 | 117.6 | 64.4 | 4 | 122.4 | 69.8 |
| 5 | 110.8 | 59.6 | 5 | 120 | 70 |
| 6 | 104.6 | 55.5 | 6 | 117.7 | 70.2 |

at three different methane flow rates. Increasing pressures allow a higher rate of hydrogen to be recovered in permeation zone and thus higher volumetric flow rates of pure hydrogen to be obtained. On the basis of these results and of the negligible effect of $P$ on $X_{CH_4}$ we can conclude that a high pressure has a positive effect on MR performance.

### 3.3. Effect of steam to carbon ratio

The effect of steam to carbon ratio (S/C) has been studied by two different approaches:

(1) methane inlet flow rate is fixed (5 kmol/h);
(2) space velocity is kept constant (2.45 kg/(h $kg_{cat}$)).

The results are shown in Fig. 6 and in Table 8.

The steam to carbon ratio has a positive effect on reforming and water gas shift reactions: the effect is more pronounced if the space velocity is fixed because of the unavoidable increase of overall inlet flow rate and consequent reduction of residence time with steam to carbon ratio at fixed $F^{in}_{CH_4}$. At the same time, increasing steam to carbon ratio reduces hydrogen partial pressure in the reaction zone and, then, the pure $H_2$ flow rate recovered (Table 8).

In conclusion, high S/C values allow a better performance to be obtained in terms of reaction but a worse in terms of separation. Therefore, an intermediate value of S/C has to be set as a suitable condition between these opposite effects, checking that coke formation is prevented in the reaction zone.

## 4. Conclusions

The two-dimensional model is an useful mean to simulate the behaviour of large-scale MR. In particular, it is able to explain the improvement in integrating the Pd-based membrane into the reformer in terms of two radial effects: promotion of reaction rate by temperature near the hot wall and improvement by $H_2$ removal in the central zone where catalyst temperature is not high enough. The model highlights that methane conversion is far from unit at industrial operating conditions where high flow rates have to be processed and, therefore, short residence times are involved. Moreover, the moderate thermal level required from membrane thermal instability has a bad influence on steam reforming reaction and Pd–Ag permeability. The main advantages of membrane reactors in steam reforming processes are methane conversion larger than in TR due to hydrogen removal during reaction and the production of extra-pure $H_2$. The unconverted methane and unpermeated hydrogen kept in reaction gas could be burnt to satisfy part of the heat duty of the process (heat transferred to the reformer, steam production, etc.). Some disadvantages of membrane reformer are the higher amount of steam requested by the process and the low pressure at which hydrogen flows out and consequently the necessity of using a compressor to store it. In any case, a wider industrial use of membrane reforming process depends on improvements in membrane technology, i.e. on the future availability of better materials in terms of permeability, stability, cost and separation efficiency. Moreover, MR performance depends on its geometric design as well as on heat flux profile along the reactor. An analysis of these effects has not been tackled in this work but it appears to be basic for an optimal application of membrane reforming technology and it will be the subject for future research.

## Acknowledgement

This work has been carried out within the framework of the project "Pure hydrogen from natural gas through reforming up to total conversion obtained by integrating chemical reaction and membrane separation", financially supported by MIUR (FISR DM 17/12/2002).

## References

[1] I. Dybkjaer, Tubular reforming and autothermal reforming of natural gas—an overview of available processes, Fuel Process. Technol. 42 (1995) 85–107.
[2] J. Shu, B. Grandjean, S. Kaliaguine, Catalytic palladium-based membrane reactors: a review, Can. J. Chem. Eng. 69 (5) (1991) 1036–1060.
[3] Y. Lin, S. Liu, C. Chuang, Y. Chu, Effect of incipient removal of hydrogen through palladium membrane on the conversion of methane steam reforming: experimental and modeling, Catal. Today 82 (2003) 127–139.
[4] F. Gallucci, L. Paturzo, A. Basile, A simulation study of steam reforming of methane in a dense tubular membrane reactor, Int. J. Hydrogen Energy 29 (2004) 611–617.
[5] J. Oklany, K. Hou, R. Hughes, A simulative comparison of dense and microporous membrane reactors for the steam reforming of methane, Appl. Catal. A: Gen. 170 (1998) 13–22.
[6] J. Kim, B. Choi, J. Yi, Modified simulation of methane steam reforming in Pd-membrane-packed bed type reactor, J. Chem. Eng. Jpn. 32 (1999) 760–769.
[7] G. Madia, G. Barbieri, E. Drioli, Theoretical and experimental analysis of methane steam reforming in a membrane reactor, Can. J. Chem. Eng. 77 (1999) 698–706.
[8] G. Marigliano, G. Barbieri, E. Drioli, Effect of energy transport on a palladium-based membrane reactor for methane steam reforming process, Catal. Today 67 (2001) 85–99.
[9] W. Yu, T. Ohmori, T. Yamamoto, E. Endo, T. Nakaiwa, T. Hayakawa, N. Itoh, Simulation of a porous ceramic membrane reactor for hydrogen production, Int. J. Hydrogen Energy 30 (2005) 1071–1079.
[10] M. De Falco, L. Di Paola, L. Marrelli, Heat transfer and hydrogen permeability in modeling industrial membrane reactors for methane steam reforming, Int. J. Hydrogen Energy, Submitted for publication.
[11] F. Fernandez, A. Soares Jr., Methane steam reforming modeling in a palladium membrane reactor, Fuel 85 (2006) 569–573.
[12] M. Koukou, N. Papayannakos, N. Markatos, On the importance of non-ideal flow effects in the operation of industrial-scale adiabatic membrane reactors, Chem. Eng. J. 83 (2001) 95–105.
[13] C. Fukuhara, A. Igarashi, Two-dimensional simulation of a membrane reactor for dehydrogenation of ethylbenzene, considering heat and mass transfer, J. Chem. Eng. Jpn. 36 (5) (2003) 530–539.
[14] S. Assabumrungrat, K. Suksomboom, P. Praserthdam, T. Tagawa, S. Goto, Simulation of palladium membrane reactor for dehydrogenation of ethylbenzene, J. Chem. Eng. Jpn. 35 (3) (2002) 263–273.
[15] J. Xu, G. Froment, Methane steam reforming, methanation and water-gas shift. I. Intrinsic kinetics, AIChE J. 35 (1) (1989) 88–96.
[16] J. Rostrup-Nielsen, Production of synthesis gas, Catal. Today 18 (1993) 305–324.
[17] J. Xu, G. Froment, Methane steam reforming. II. Diffusional limitations and reactor simulation, AIChE J. 35 (1) (1989) 97–103.
[18] B. Kulkarni, L. Doraiswamy, Estimation of effective transport properties in packed bed reactors, Catal. Rev.: Sci. Eng. 22 (3) (1980) 431–483.

[19] S. Sandler, Chemical and Engineering Thermodynamics, 3rd ed., John Wiley and Sons, 1999.
[20] R. Perry, D. Green, J. Maloney, Perry's Chemical Engineers' Handbook, 6th ed., McGraw Hill, New York, 1984.
[21] R. Reid, J. Prausnitz, B. Poling, The Properties of Gases and Liquids, 4th ed., McGraw Hill, New York, 1988.
[22] A. Lindsay, A. Bromley, Ind. Eng. Chem. 42 (1950) 1508.
[23] A. Wassiljewa, Phys. Z. 5 (1904) 737.
[24] E. Tsotsas, E. Schlünder, Heat transfer in packed beds with fluid flow: remarks on the meaning and the calculation of a heat transfer coefficient at the wall, Chem. Eng. Sci. 45 (1990) 819–837.
[25] C. Li, B. Finlayson, Heat transfer in packed beds—a revaluation, Chem. Eng. Sci.
[26] R. Perry, D. Green, J. Maloney, Perry's Chemical Engineers' Handbook, 7th ed., McGraw Hill, New York, 1999.
[27] A. De Wasch, G. Froment, Heat transfer in packed beds, Chem. Eng. Sci. 27 (1972) 567–576.
[28] S. Elnashaie, S. Elshishini, Modelling, simulation and optimization of industrial fixed bed catalytic reactors Topics in Chemical Engineering, vol. 7, Gordon and Breach Science Publisher, 1993.
[29] D. Kunii, J. Smith, Heat transfer characteristics of porous rocks, AIChE J. 6 (1) (1960) 71–78.
[30] S. Yagi, D. Kunii, Studies on effective thermal conductivities in packed beds, AIChE J. 3 (3) (1957) 373–380.
[31] B. Morreale, M. Ciocco, R.M. Enick, B. Morsi, B. Howard, A. Cugini, K. Rothernberger, The permeability of hydrogen in bulk palladium at elevated temperatures and pressures, J. Membr. Sci. 212 (2003) 87–97.
[32] A. Basile, L. Paturzo, A. Vazzana, Membrane reactor for the production of hydrogen and higher hydrocarbons from methane over $Ru/Al_2O_3$ catalyst, Chem. Eng. J. 93 (2003) 31–39.
[33] J. Shu, B. Grandjean, S. Kaliaguine, Methane steam reforming in asymmetric Pd and Pd–Ag porous SS membrane reactors, Appl. Catal. A: Gen. 119 (1994) 305–325.
[34] M. Pedernera, J. Pina, O. Daniel, V. Bucalà, Use of a heterogeneous two-dimensional model to improve the primary steam reformer performance, Chem. Eng. J. 94, 29–40.
[35] J. Rajesh, S. Gupta, G. Rangaiah, A. Ray, Multiobjective optimization of steam reformer performance using genetic algorithm, Ind. Eng. Chem. Res. 39 (2000) 706–717.
[36] J. Tong, Y. Matsumura, Pure hydrogen production by methane steam reforming with hydrogen-permeable membrane reactor, Catal. Today 111 (2006) 147–152.